Materials Research Express

PAPER

Investigation of the mechanical properties of Ni-B/hBN composite coatings electrodeposited in presence of CTAB as the surfactant

To cite this article: Ali Tozar and smail H Karahan 2019 *Mater. Res. Express* **6** 126598

View the article online for updates and enhancements.

IOP ebooks™

Bringing you innovative digital publishing with leading voices to create your essential collection of books in STEM research.

Start exploring the collection - download the first chapter of every title for free.

This content was downloaded from IP address 128.59.222.107 on 06/12/2019 at 04:11

Materials Research Express

RECEIVED
18 September 2019

REVISED
31 October 2019

ACCEPTED FOR PUBLICATION
27 November 2019

PUBLISHED
6 December 2019

PAPER

Investigation of the mechanical properties of Ni-B/hBN composite coatings electrodeposited in presence of CTAB as the surfactant

Ali Tozar[1] and İsmail H Karahan[1,2]

[1] Mustafa Kemal University, Faculty of Arts and Science, Department of Physics, Hatay, Turkey
[2] University of North Texas, Department of Chemistry, Denton, United States of America

E-mail: tozarali@gmail.com and tozarali@mku.edu.tr

Keywords: Ni-B, composite coating, electrodeposition, nanoindentation, wear, friction

Abstract

The effect of hexadecyltrimethylammonium bromide (CTAB) concentration on the galvanostatic electrodeposition of Ni-B matrix nano hexagonal boron nitride (hBN) reinforced composite coatings was investigated. XRD and FE-SEM analyzes were used for crystallographical and morphological investigations, respectively. Vickers indentation, nanoindentation, and nanoscratch experiments were carried out to investigate the micromechanical, nanomechanical and tribological properties, respectively. Potentiodynamic polarization and electrochemical impedance spectroscopy techniques were applied for corrosion characterization. The investigated properties have been improved with the increasing CTAB concentrations up to 900 μM. In a general manner, CTAB has a beneficial effect at lower concentrations and can be useful for metal matrix nano ceramic reinforced composite coating electrodeposition in the lower concentration range.

1. Introduction

Due to their favorable properties such as high mechanical endurance (Vitry *et al* 2019), good corrosion resistance (Salehikahrizsangi *et al* 2018) and, cost-effectiveness, engineering design nickel and nickel alloy coatings have been used in industry for nearly a century. Electrolytic and electroless deposition are the most preferred techniques in the industry because of their ease and variety of application. Nickel-based coatings continue to be developed in line with the specific needs and demands of each industrial sector. For instance, Ni-B coatings have been developed for the high corrosion (Li *et al* 2018), mechanical (Matsui *et al* 2018) and tribological (Mukhopadhyay *et al* 2018) resistance demands of automotive, aerospace and chemical engineering sectors.

Due to the need of high temperatures (Mukhopadhyay *et al* 2017) and pH (Srinivasan *et al* 2010) values and the strict stabilization of these parameters for electroless deposition, electrodeposition seems more feasible for the deposition of Ni-B coatings (Hu *et al* 2019). Therefore, the electrodeposition of Ni-B alloys is a popular subject of recent years (Ogihara *et al* 2011, Kwon *et al* 2017, Matsui *et al* 2018). Improving corrosion protection performance (Shakoor *et al* 2017b) and enhancement of hardness (Shakoor *et al* 2017a) are the main themes of these studies. There are studies that revealing positive results in terms of mechanical properties by heat treatment of Ni-B coatings (Lee *et al* 2005, Pal *et al* 2011). However, it is a compelling fact that heat treatment reduces the corrosion resistance by causing micro cracks on the coating. Electrodeposition of nickel matrix composite coating reinforced with nano-ceramic particles is seen as a promising advance in order to overcome this problem.

In recent years, many studies have been carried out in which Ni-B alloys have been electrodeposited with different ceramics such as SiC (Mehr *et al* 2019), Y_2O_3 (Shakoor *et al* 2017a), V_2O_5 (Waware *et al* 2018), and ZrO_2 (Shakoor *et al* 2015) and hBN (Unal and Karahan 2018b) for obtaining composite materials. Among these, hBN is remarkable for its mechanical strength as well as its solid lubrication and wide use of potential (Tozar and Karahan 2018a, 2018b, Tozar *et al* 2019). Therefore hBN attracts the attention of the researchers interested in the electrodeposition of composite coatings (Tudela *et al* 2015, Unal and Karahan 2018a).

© 2019 IOP Publishing Ltd

Table 1. Electrodeposition conditions of the composite coatings.

Chemical	Concentration
$NiSO_4.6H_2O$	250 g.l^{-1}
$NiCl_2.6H_2O$	55 g.l^{-1}
H_3BO_3	35 g.l^{-1}
TMAB	6 g.l^{-1}
hBN	12 g.l^{-1}
CTAB	0. 300. 600. 900. 1500 μM
Operating conditions	
Temperature	43 °C
pH	4
Deposition current density	50 mA.cm^{-2}
Deposition time	60 min.
Agitation speed	250 rpm

There are many parameters affecting the electrodeposition such as current density (Maharana *et al* 2019), pH (Liu *et al* 2019), temperature (Elsayed *et al* 2019), additive type (Ning *et al* 2019), and concentration (Dheeraj *et al* 2017) etc. Especially using surfactants as additive has an enormous effect on composite electrodeposition (Afroukhteh *et al* 2012, Gyawali *et al* 2014). As a cationic surfactant cetyltrimethylammonium bromide (CTAB) exhibits significant property changes on electrodeposited composite films (Faridi *et al* 2017, Kan *et al* 2018). Although the effect of CTAB on the electrodeposition of nickel matrix composite reinforced by some ceramics such as CNTs (Guo *et al* 2008) and, SiC (Rudnik *et al* 2010) has been investigated, there is not a single study regarding Ni-B/hBN composite coatings. In this study, Ni-B/hBN composite coatings were fabricated by the galvanostatic electrodeposition technique and the effect of CTAB concentration on the structural, mechanical and corrosion protection properties of the electrodeposited coatings were investigated.

2. Experimental

The Ni-B/hBN composite coatings were fabricated by the galvanostatic electrodeposition method using a Watt type bath with varying CTAB concentrations. Operating conditions and concentrations of the ingredients are given in table 1. The average particle size of hBN was 100 nm. All the electrochemical synthesis and analysis were conducted in a glass beaker of 250 ml volume with a CHI 608 model electrochemical analyzer. The reference electrode was saturated calomel, the counter electrode was a platinum wire, the working electrode was a 304 L grade steel sheet and the distance between the working and counter electrode was kept 50 mm. All the deposition suspensions were freshly prepared by double distilled water and subjected to ultrasonic agitation as described elsewhere (Unal and Karahan 2018a).

Crystallographic structures of the coatings were examined by x-ray diffraction method using a Rigaku x-ray diffractometer. XRD scans were conducted with the CuK_α radiation obtained at 40 kV and 30 mA. The scan rate was 3.0 deg min^{-1} and the grazing incidence was 5 degrees. Surface morphology and elemental composition of the coatings were investigated via field emission scanning electron microscopy (FE-SEM) by an energy dispersive x-ray spectrometer (EDS) attached Apreo-S model FE-SEM.

X-Ray diffraction planes matched by using the 01-079-6756, 01-079-2916 00-004-0850 ICDD cards. In order to quantitatively estimate the preferred orientation of the Ni-B matrix, relative texture coefficient RTC (hkl) values were calculated by the following equation (Gu *et al* 2018);

$$\%RTC(hkl) = \frac{TC(hkl)}{\sum TC(hkl)} \tag{1}$$

Where TC(hkl) is the texture coefficient of (hkl) plane and $\sum TC(hkl)$ is the sum of all texture coefficient of all planes in the pattern. Texture coefficient of a (hkl) plane is defined as (Yousif *et al* 2017);

$$TC(hkl) = \frac{\mathrm{I}(hkl)}{\sum \mathrm{I}(hkl)} x \frac{\sum \mathrm{I}_0(hkl)}{\mathrm{I}_0(hkl)} \tag{2}$$

Where I(hkl) is the intensity of the peak corresponding to (hkl) plane, $\sum I(hkl)$ is the sum of all intensities in the pattern, I_0(hkl) is the intensity of the peak of (hkl) plane in the reference card.

Micromechanical characterization of the coatings was conducted via a Vickers microhardness instrument with a load of 1 kgf. Nanomechanical and wear characteristics were examined by a Hysitron TI 950™ triboindenter with an attached Berkovich tip with the diameter of 150 nm and the half-angle of 65.35° between the three sides of the pyramid. 3 × 3 grid formation nanoindentations were carried out to all coatings using a trapezoidal load function (5 s of loading, 2 s of constant maximum force and 5 s of unloading) with a maximum force of 5000 μN. The elastic modulus (E_r) and hardness (H) values of the samples were determined from the unloading curves by the methods specified in the literature (Oliver and Pharr 2011, Díez-Pascual *et al* 2015). Nanoscratch tests were performed with special 9 segments load function having a maximum load of 5000 μN. And, the scratch length was 10 μm with a speed of 0.25 $\mu m.s^{-1}$. The coefficient of friction (CoF) of the coatings was calculated from the following equation (Bhushan 2008).

$$CoF = \frac{Latheral\ Froce\ (LF)}{Normal\ Force\ (NF)} \tag{3}$$

Maximum load segments were used for the calculation. Surface topography images of the coatings were recorded via scanning probe microscopy (SPM). The average surface roughness and wear volume of the coatings were calculated by the Gwyddion 2.48 software.

Corrosion protection characteristics of the coatings were investigated with Tafel extrapolation and electrochemical impedance spectroscopy techniques using a %3.5 wt NaCl solution. Tafel experiments were carried out with the potential range of −0.25–1 V versus open circuit potential and the scan rate of 1 $mV.s^{-1}$. EIS studies were carried out at a frequency range of 100 kHz–10 mHz (10^5–10^{-2} Hz) with a 10 mV amplitude AC signal.

3. Results and discussion

XRD patterns and RTC plots of the coatings have been shown in figures 1(a), and (b), respectively. As it is seen from the XRD patterns, that Ni crystalized mainly through the (220), (200) and, (110) directions. Although they are overlapped with Ni peaks, the (130) and (221) peaks belong to Ni-B alloy can be determined from the ICDD reference data. According to RTC plot, the relative texture coefficient of the (110) plane has been increased with the increasing CTAB concentrations up to 900 μM and then decreased with an excessive increase up to 1500 μM. On the other hand, RTC of (200) and (220) directions showed the opposite behavior in general. Although the preferred orientation of electrodeposited Ni is majorly connected to deposition conditions (Ogihara *et al* 2012), preferred orientation pattern of the matrix has not been changed with the increasing CTAB concentrations. This phenomenon has been attributed to adsorbed species included in the deposition bath by some researchers (Amblard *et al* 1979, Amblard *et al* 1983). Another observation that can be made from the XRD patterns is that the peaks of the preferred crystallization orientations are quite broad, which results in the coatings having a very small-grained structure at about 10 nm. Also, the occurrence of the amorphous shoulder at low 2 theta values and the accompanying intensity increase of the peak corresponding to (002) direction of hBN with increasing CTAB concentrations can be seen. This may also affect the texture of the Ni matrix.

FE-SEM images of the coatings have been shown in figure 2. As it is seen from the figure that the surface morphologies of the coatings have been significantly altered when CTAB added to deposition suspension. Although tuber-like structures resulting from the nucleation of nickel in different regions can be obviously recognized, it can be said that with increasing CTAB concentrations, the coating surface generally has become flatter and more compact. It can also be said that partly irregular clusters have occurred on the coating surface produced at 1500 μM CTAB concentration. Another noteworthy observation from the FE-SEM images was the texture-like structural formations, especially on the coating surfaces produced at the concentrations of 300 and 600 μM. As an interesting observation supporting this heterogenetic surface structure of the coating electrodeposited with 600 μM CTAB concentration, figure 3 shows the post indentation optical image of two indents applied in the same direction. As can be seen from the figure the two different regions have shown two different deformation behavior under the load. The indent at the left side has shown a plastic flow behavior while the indent at the right side has been shown pile-up behavior. This may be attributed to releasing of the residual stress and strain around the indentation area due to plastic tensile stress (Ma *et al* 2015). From surface morphologies, it can be seen that distribution of the reinforcement particles is regularized with increasing CTAB concentrations up to 900 μM and unregularized with further increase.

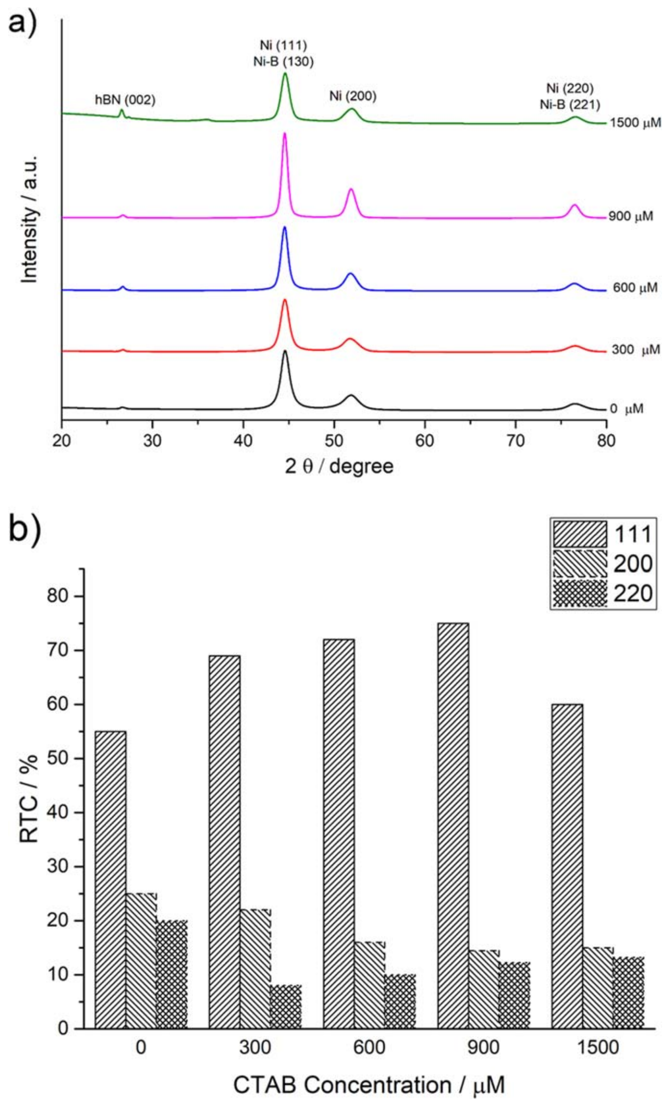

Figure 1. XRD spectra (a) and RTC % graph (b) of the coatings electrodeposited with increasing CTAB concentrations.

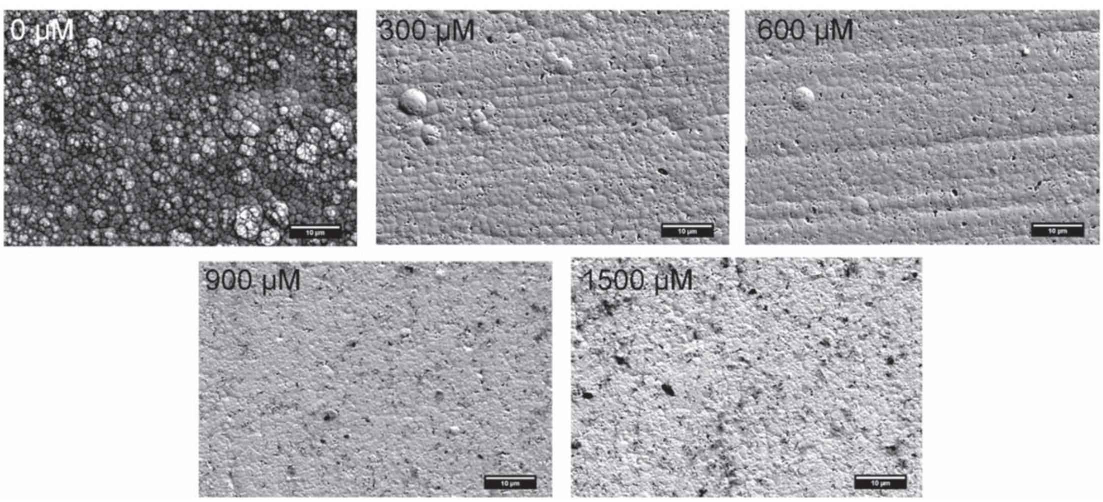

Figure 2. Surface morphology FE-SEM images of the coatings electrodeposited with increasing CTAB concentrations.

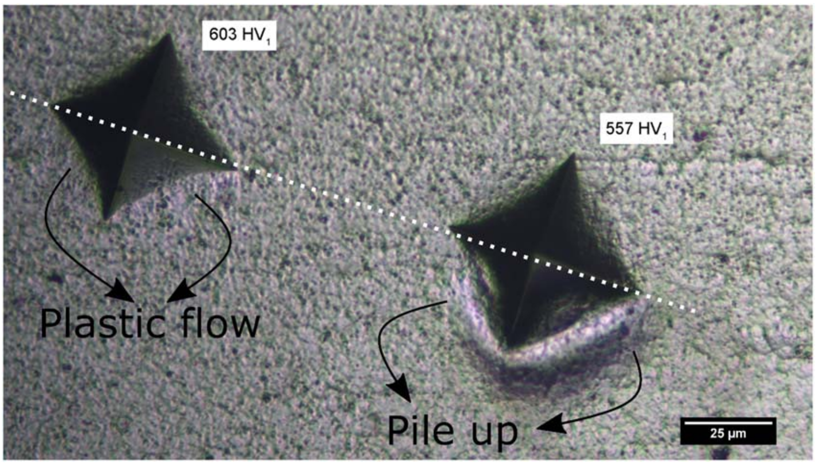

Figure 3. Optical images of the two microindentions showing different deformation behavior (image belongs coating electrodeposited with 600 μM CTAB concentration).

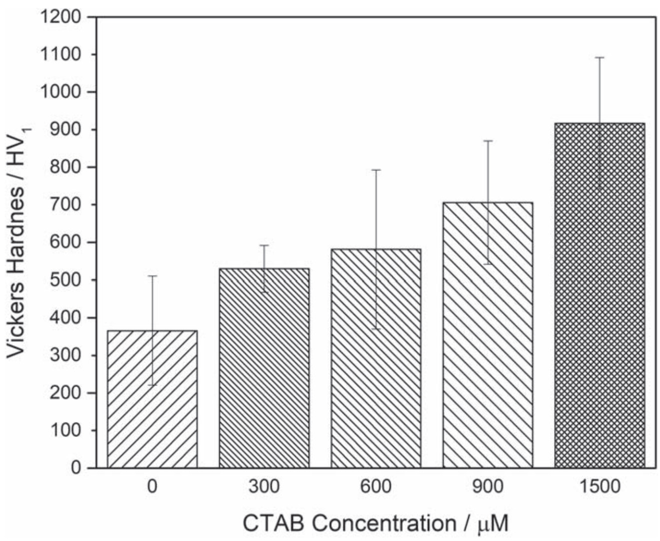

Figure 4. Vickers hardness values of the coatings electrodeposited with increasing CTAB concentrations.

Vickers microhardness value plots of the coatings have been shown in figure 4. As it is seen from the plot that HV_1 has been regularly increased with the increasing CTAB concentrations. With the mean HV_1 value of 917, the coating electrodeposited with 1500 μM has the highest Vickers microhardness value. This regular increase may be attributed to the hBN content in the coating with the increasing CTAB concentrations. However, the HV_1 values of the coatings except the coating produced with 300 μM CTAB concentration have a relatively high standard deviation value due to exceedingly varying values through the coating surface.

The nanoindentation load-displacement curves have been presented in the figure 5. Nine indentations have been applied to each coating with a 3×3 grid formation. In order to see the distribution of E_r and H values obtained from the load-displacement curves, the statistical projection has been presented in box graph form in the figures 6(a) and (b), respectively.

Pop-in behaviors indicating rapid displacement for all coatings except those produced with 600 and 900 μM CTAB concentration can be seen from the load-displacement curves. These pop-ins may be due to the indentation size effect which may originate from surface roughness for coatings produced at low CTAB concentrations. On the other hand, for coating produced at 1500 μM CTAB concentration, pop-ins can be thought to occur due to agglomerations of hBN particles.

As can be seen from the box graphs of the coatings produced at very low and very high CTAB concentrations, a high distribution was observed in the E_r values compared to the coatings produced at medium values

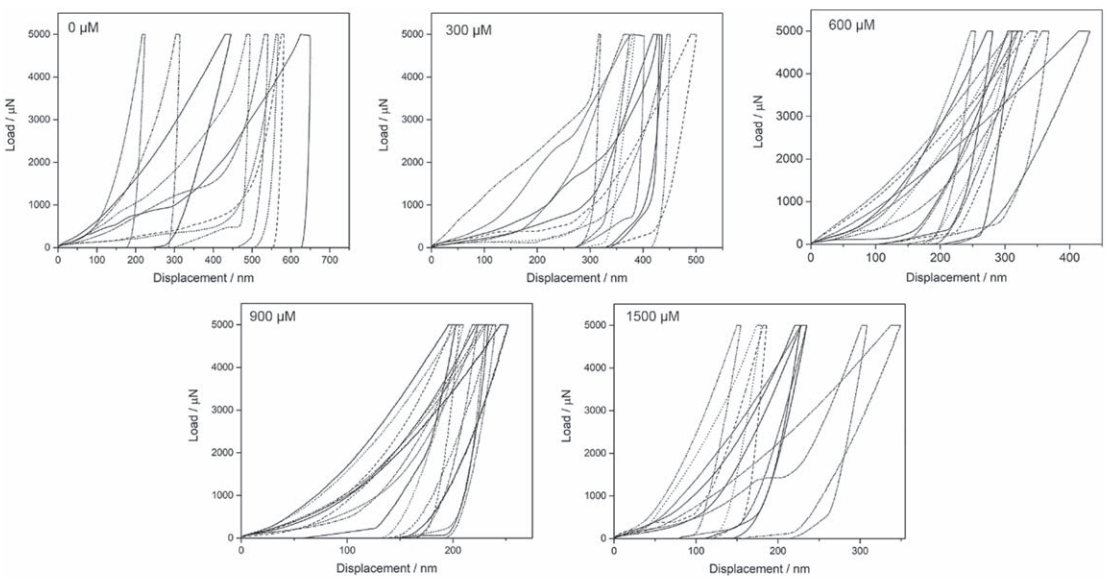

Figure 5. Load-displacement curves of the coatings electrodeposited with increasing CTAB concentrations.

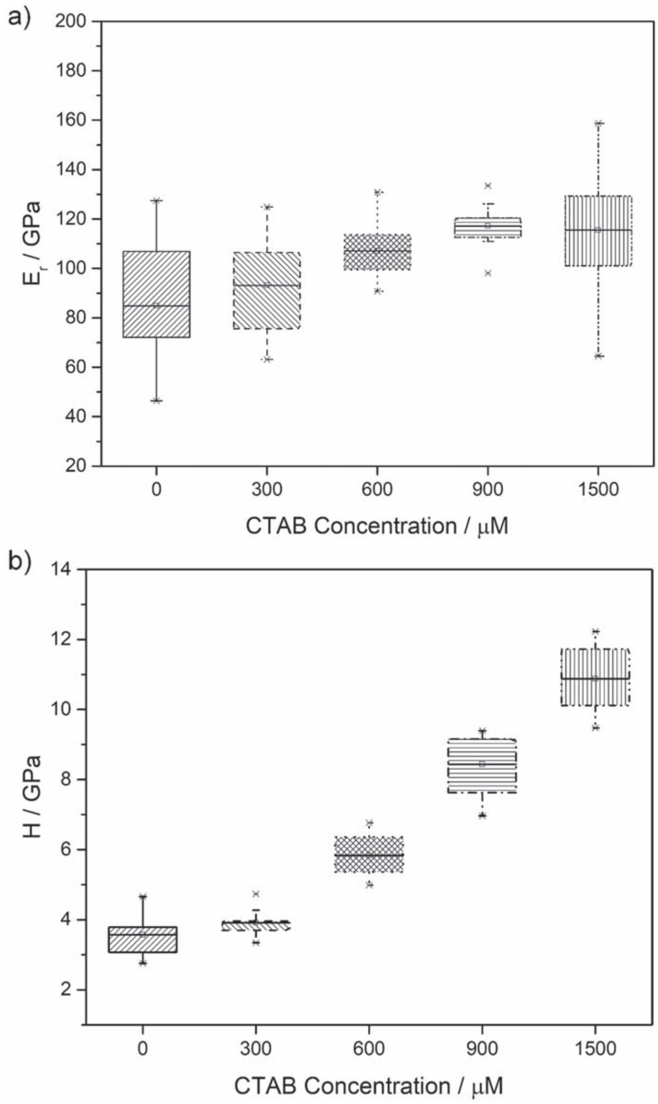

Figure 6. Elastic modulus (b) and Hardness (c) box graphs obtained from the statistical evaluation of nanoindentation tests.

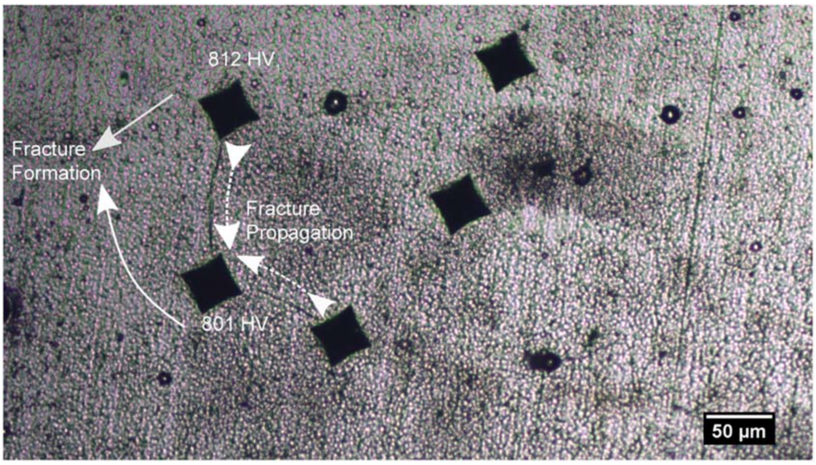

Figure 7. Optical images showing fracture formation and propagation on the coating electrodeposited with 1500 μM CTAB concentration.

(600 and 900 μM). On the other hand, the same situation has not been observed for H. While the H values have been increased very rapidly with the increase in the CTAB concentration, the E_r value has not been increased at the same rate and even the average E_r value for the coating produced at 1500 μM has remained almost the same. It can be concluded that the coatings have become more brittle with the increasing CTAB concentrations. It can even be said that the irregularities observed in the load-displacement curves may be originated from this non-parallel increase between the H and E_r. This may cause a coating to be more brittle. As a supporting observation, figure 7 shows an optical image of the coating produced with 1500 μM CTAB concentration. Fracture formation and propagation towards neighbor indent can be observed from the figure. Although the H value of the coatings has been increased, this change has occurred in a brittle manner due to the mismatch between the increase of E_r and H values. The coating produced with 900 μM has the highest mean E_r value of 117 GPa. On the other hand, the coating produced with 1500 μM has the highest mean H value of 10.87 GPa. The results obtained from nanohardness tests and Vickers microhardness tests show similarities.

The coefficient of friction (CoF) values obtained with dividing lateral force to normal force of the constant loading segment of the nanoscratch tests and their corresponding average values have been presented in figures 8(a) and (b), respectively. As it is seen from the CoF curves that there are some rapid increase and decrease regions for the coatings obtained at the CTAB concentrations of 0 and 1500 μM. These regions may be due to the crack formations originated from the changeover of areas of varying H and E_r on the surface of the coating. This indicates that the mechanical properties at this coating surface can be quite variable due to the irregular distribution of hBN particles. However, when the results are evaluated on average values, it can be said that the friction coefficient of the coatings is decreased with increasing CTAB concentrations up to 900 μM and remains nearly constant with further increase.

The wear behaviors of the coatings are investigated via SPM imaging and given in figure 9. As can be seen from the figure that there is a remarkable change in the wear scars of the coatings with the increasing CTAB concentrations. In general, it can be said that there is a tendency towards narrowing and smoothening. However, for the coating produced at the concentration of 1500 μM, the obvious difference between the sides of the valley is drawn attention. As such, it is similar to the coating produced without CTAB. For wear volumes calculated for scars, it can be said that wear volume decreases with increasing CTAB concentrations.

A summary of the results of nanomechanical and tribological results of the coatings can be found in figure 10 and table 2. As can be seen, with the increase of CTAB concentration there is an increase in the hBN volume fraction in the coating. With regard to this, an increase in the E_r and H values. However, the E_r value has continued to be increased with increasing CTAB concentration up to 900 μM, it has been decreased with further increase. On the other hand, wear volume of the scratches has been decreased with the increase of the hBN volume fraction in the coating. Similar to E_r, CoF values have been decreased with CTAB concentration up to 900 μM, it has been increased with further increase. This difference between the changing rate of these four properties, which are tightly connected to each other, can be attributed to the irregularity in the distribution of the reinforcement particles. It can be said that CTAB enhances both the volume fraction of the reinforcement particles and their distribution up to a certain

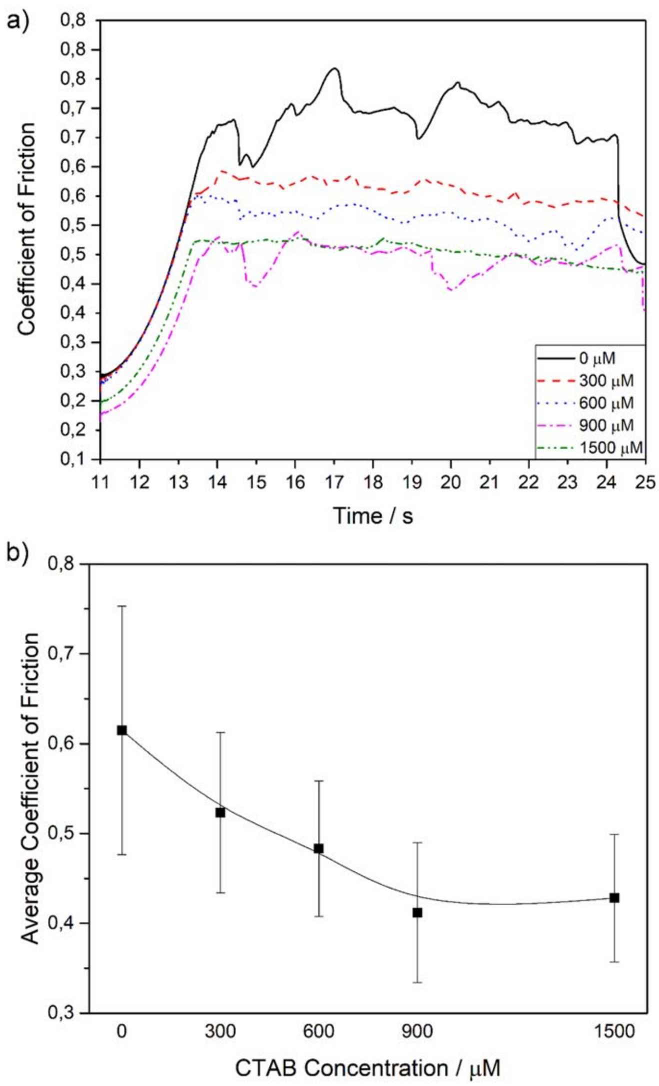

Figure 8. CoF values during the nanoscratch test (a) and average CoF values of the coatings electrodeposited with increasing CTAB concentrations.

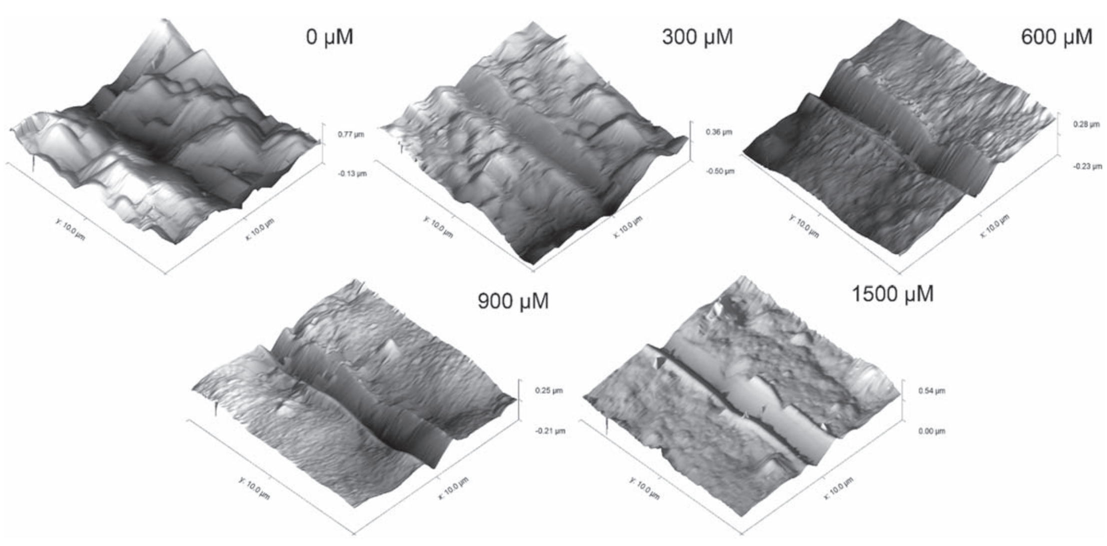

Figure 9. 3D SPM images of the wear scars obtained after nanoscratch tests.

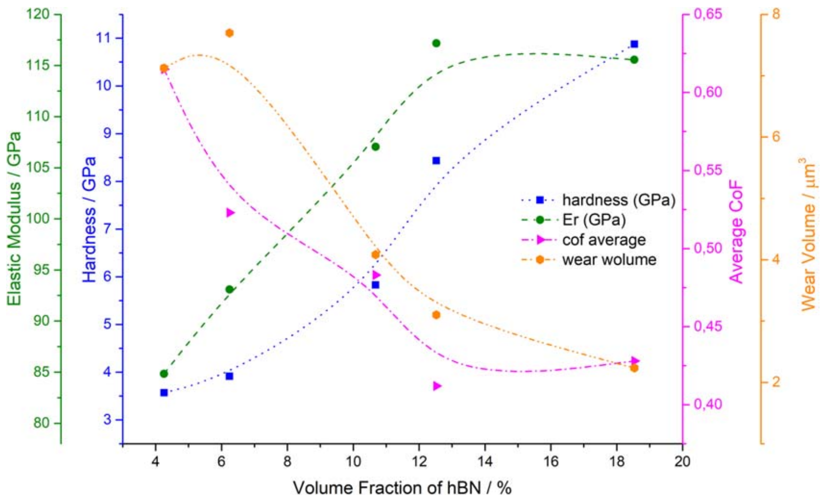

Figure 10. Summary of the relation between mechanical and tribological properties and volume fraction of the reinforcement ceramic in the coatings.

concentration and worsens with further increases. Our findings resemble with the study made by Kılıç *et al* (Kılıç *et al* 2013).

Tafel and impedance modulus plots of the coatings and uncoated steel recorded in 3.5%wt. NaCl can be found in figures 11(a) and (b), respectively. As can be seen from the Tafel curves that the E_{corr} values of the coatings have been located to the nobler side of the bare steel. This indicates the barrier protection mechanism. On the other hand, the E_{corr} values have increased with the increasing CTAB concentration up to 900 μM and decreased with further increase. This indicates the deterioration of the barrier properties of the coating. It can be attributed to the formation of pores due to the agglomeration of the reinforcement particles. In the modulus plot of the respective coating, the decrease in the modulus value at the low-frequency region supports the conclusion that the coating has deteriorated barrier properties. It can easily be said that with the noblest E_{corr} value of -0.38 V and the higher modulus values through all frequency regions, the coating electrodeposited with the CTAB concentration of 900 μM has protected steel best among all coatings. The increasing volume fraction of the reinforcement particles up to a certain value improved the corrosion protection properties and then started to be deteriorated with further increase due to irregular distribution.

4. Conclusions

The electrodeposition of hBN reinforced Ni-B matrix composite coatings on steel sheets has been successfully carried out. Hexadecyltrimethylammonium bromide (CTAB) has been used as the cationic surfactant. The effect of the CTAB concentration on the properties of electrodeposited composite coatings has been investigated. It can be concluded that up to a certain concentration (900 μM) CTAB shows a beneficial effect on the mechanical and corrosion protection properties thanks to its good dispersive effect on the reinforcement particles. However, this beneficial effect has been started to be inverted with excessive CTAB concentrations (1500 μM) due to the agglomeration of the reinforcement particles. The character of the suspension has started to be changed with excessive CTAB concentrations. Too much foaming on the suspension surface and accompanying agglomerations of the particles in the suspensions have started to be observed for 1500 μM CTAB concentration. Although the hardness value of the coatings has been increased, this change has occurred in a brittle manner due to the mismatch between the increase of elastic modulus and hardness values. Moreover, in the trial films electrodeposited over 1500 μM, spallings, peelings, and crackings were observed due to internal stress, and adhesion problems. This may be caused by the increasing brittleness. It can be concluded that CTAB can effectively be used with the very low concentrations for electrodeposition of ceramic reinforced metal matrix composites.

Table 2. A summary of the investigated properties.

CTAB Concentration (μM)	Volume Fraction of hBN particle (%)	Microhardness (HV_1)	Hardness (H) (GPa)	Elastic Modulus (E_r) (GPa)	Coefficient of Friction (CoF)	Wear Volume (μm^3)	Average Surface Roughness (R_a) nm	Corrosion Potential (E_{corr}) (V)	Corrosion Rate (mmpy)
0	4.25	365	3.57	84.84	0.614	7.123	154	−0.545	3.924
300	6.24	530	3.91	93.08	0.523	7.697	117	−0.512	1.470
600	10.68	581	5.83	107.04	0.483	4.083	80	−0.490	0.545
900	12.53	706	8.43	117.17	0.412	3.101	59	−0.380	0.306
1500	18.54	917	10.88	115.55	0.428	2.235	42	−0.420	0.432

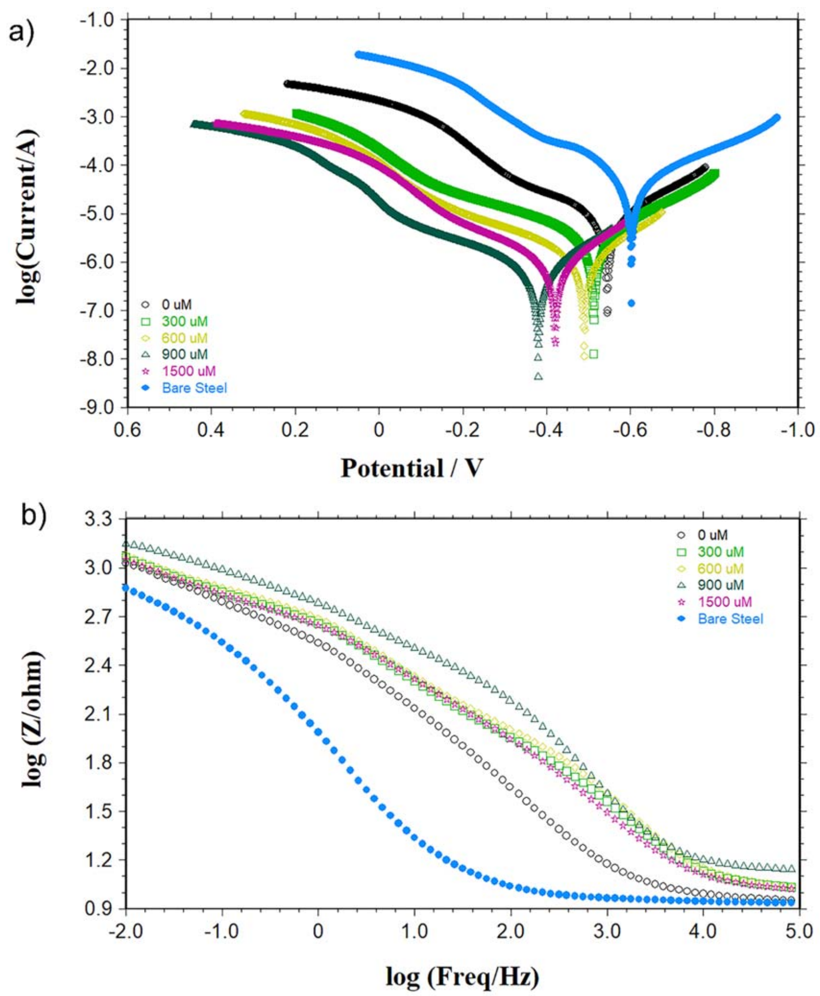

Figure 11. Tafel curves (a) and impedance modulus plot (b) of the coatings electrodeposited with increasing CTAB concentrations.

Acknowledgments

Special thanks to Mustafa Kemal University Scientific Research Projects for the financial support (Project No. 19 M 020).

ORCID iDs

Ali Tozar https://orcid.org/0000-0003-3039-1834

References

Afroukhteh S, Dehghanian C and Emamy M 2012 Corrosion behavior of Ni–P/nano-TiC composite coating prepared in electroless baths containing different types of surfactant *Progress in Natural Science: Materials International* **22** 480–7

Amblard J, Epelboin I, Froment M and Maurin G 1979 Inhibition and nickel electrocrystallization *J. Appl. Electrochem.* **9** 233–42

Amblard J, Froment M, Maurin G, Spyrellis N and Trevisan-Souteyrand E 1983 Nickel electrocrystallization—from nucleation to textures *Electrochim. Acta* **28** 909–15

Bhushan B 2008 *Nanotribology and Nanomechanics: An Introduction* (Berlin Heidelberg: Springer) (https://doi.org/10.1007/978-3-540-77608-6)

Dheeraj P R, Patra A, Sengupta S, Das S and Das K 2017 Synergistic effect of peak current density and nature of surfactant on microstructure, mechanical and electrochemical properties of pulsed electrodeposited Ni-Co-SiC nanocomposites *Journal of Alloys and Compounds,* **729** 1093–107

Díez-Pascual A M, Gómez-Fatou M A, Ania F and Flores A 2015 Nanoindentation in polymer nanocomposites *Prog. Mater Sci.* **67** 1–94

Elsayed E M, Rashad M M, Ibrahim I A, Hussein M R and El-Sabbah M M B 2019 Electrochemical synthesis of nanocrystalline $NiFe_2O_4$ thin film from aqueous sulphate bath *J. Alloys Compd.* **798** 104–11

Faridi M, Nari A, Kalhor H and Dadjoo M H 2017 A comparative study on Ag-doped and surfactant assisted MnO_2 prepared by direct and pulse current electrodeposition on surgical grade stainless steel as high-performance supercapacitor *J. Braz. Chem. Soc.* **28** 168–78

Gu W, Liu C, Tang J, Liu R, Yang H and Hu J 2018 Improving zinc electrodeposition in ammoniacal electrolytes with the saturated dissolved methyltrioctylammonium chloride *Hydrometallurgy* **175** 43–51
Guo C, Zuo Y, Zhao X, Zhao J and Xiong J 2008 Effects of surfactants on electrodeposition of nickel-carbon nanotubes composite coatings *Surf. Coat. Technol.* **202** 3385–90
Gyawali G, Hamal K, Joshi B, Rajbhandari A and Wohn Lee S 2014 Microstructural and electrochemical analysis of Ni–SiC composite coatings prepared in presence of additives *Materials Letters,* **126** 228–31
Hu C, Xu M, Zhang J, Hu B and Yu G 2019 High corrosion resistance of electroless Ni/Ni-B coating from fluoride-free baths on AZ31 magnesium alloy *J. Alloys Compd.* **770** 48–57
Kan H M, Feng X J, Wei X D, Zhang N, Wang X Y and Long H B 2018 Effects of surfactants SDS and CTAB on Ni-SiC deposition *Journal of Wuhan University of Technology-Materials Science Edition* **33** 836–42
Kiliç F, Gül H, Aslan S, Alp A and Akbulut H 2013 Effect of CTAB concentration in the electrolyte on the tribological properties of nanoparticle SiC reinforced Ni metal matrix composite (MMC) coatings produced by electrodeposition *Colloids Surf.* A **419** 53–60
Kwon H B, Kim K, Ahn H R and Kim Y J 2017 Electrodeposition and characterization of nanocrystalline Ni-B with low boron content for MEMS applications *Sensors and Materials* **29** 225–34
Lee K H, Chang D and Kwon S C 2005 Properties of electrodeposited nanocrystalline Ni–B alloy films *Electrochim. Acta* **50** 4538–43
Li B S, Zhang W W, Li D D, Huan Y X and Dong J 2018 Microstructural, surface and electrochemical properties of a novel Ni-B/Ni-W-BN duplex composite coating by co-electrodeposition *Appl. Surf. Sci.* **458** 305–18
Liu W N, Qiao X J, Liu S, Shi S M, Liang K and Tang L 2019 A new process for pre-treatment of electroless copper plating on the surface of mica powders with ultrasonic and nano-nickel *J. Alloys Compd.* **791** 613–20
Ma Z C, Zhao H W, Lu S, Li H L, Liu C Y and Liu X H 2015 Deformation behavior of micro-indentation defects under uniaxial and biaxial loads *Rev. Sci. Instrum.* **86** 10
Maharana H S, Bishoyi B and Basu A 2019 Current density dependent microstructure and texture evolution and related effects on properties of electrodeposited Ni-Al coating *J. Alloys Compd.* **787** 483–94
Matsui I, Omura N, Yamamoto T and Takigawa Y 2018 Electrodeposition with intermittent addition of trimethylamine borane to produce ductile bulk nanocrystalline Ni-B alloys *Surface & Coatings Technology* **337** 411–7
Mehr M S, Akbari A and Damerchi E 2019 Electrodeposited Ni-B/SiC micro- and nano-composite coatings: a comparative study *J. Alloys Compd.* **782** 477–87
Mukhopadhyay A, Barman T K and Sahoo P 2017 Effects of heat treatment on tribological behavior of electroless Ni-B coating At elevated temperatures *Surf. Rev. Lett.* **24** 22
Mukhopadhyay A, Barman T K, Sahoo P and Davim J P 2018 Comparative study of tribological behavior of electroless Ni-B, Ni-B-Mo, and Ni-B-W coatings at room and high temperatures *Lubricants* **6** 17
Ning D D, Zhang A, Murtaza M and Wu H 2019 Effect of surfactants on the electrodeposition of Cu-TiO_2 composite coatings prepared by jet electrodeposition *Journal of Alloys and Compounds* **777** 1245–50
Ogihara H, Miyamoto K, Udagawa K and Saji T 2011 Electrodeposition of super hard Ni-B/diamond composite coatings *Chem. Lett.* **40** 1072–3
Ogihara H, Udagawa K and Saji T 2012 Effect of boron content and crystalline structure on hardness in electrodeposited Ni–B alloy films *Surf. Coat. Technol.* **206** 2933–40
Oliver W C and Pharr G M 2011 An improved technique for determining hardness and elastic modulus using load and displacement sensing indentation experiments *J. Mater. Res.* **7** 1564–83
Pal S, Verma N, Jayaram V, Biswas S K and Riddle Y 2011 Characterization of phase transformation behaviour and microstructural development of electroless Ni–B *coating. Materials Science and Engineering:* A **528** 8269–76
Rudnik E, Burzyńska L, Dolasiński Ł and Misiak M 2010 Electrodeposition of nickel/SiC composites in the presence of cetyltrimethylammonium bromide *Appl. Surf. Sci.* **256** 7414–20
Salehikahrizsangi P, Raeissi K, Karimzadeh F, Calabrese L, Patane S and Proverbio E 2018 Erosion-corrosion behavior of highly hydrophobic hierarchical nickel coatings *Colloids and Surfaces a-Physicochemical and Engineering Aspects* **558** 446–54
Shakoor R A, Kahraman R, Waware U S, Wang Y X and Gao W 2015 Properties of electrodeposited Ni-B-ZrO_2 composite coatings *International Journal of Electrochemical Science* **10** 2110–9
Shakoor R A, Waware U S, Ali K, Kahraman R, Popelka A, Yusuf M M and Hasan A 2017a Novel electrodeposited Ni-B/Y_2O_3 composite coatings with improved properties *Coatings* **7** 10
Shakoor R A, Waware U S, Kahraman R, Popelka A and Yusuf M M 2017b Corrosion behavior of electrodeposited Ni-B coating modified with SiO_2 particles *Int. J. Electrochem. Sci.* **12** 4384–91
Srinivasan K N, Meenakshi R, Santhi A, Thangavelu P R and John S 2010 Studies on development of electroless Ni-B bath for corrosion resistance and wear resistance applications *Surf. Eng.* **26** 153–8
Tozar A and Karahan İ H 2018a A comparative study on the effect of collagen and h-BN reinforcement of hydroxyapatite/chitosan biocomposite coatings electrophoretically deposited on Ti-6Al-4V biomedical implants *Surf. Coat. Technol.* **340** 167–76
Tozar A and Karahan İ H 2018b A comprehensive study on electrophoretic deposition of a novel type of collagen and hexagonal boron nitride reinforced hydroxyapatite/chitosan biocomposite coating *Appl. Surf. Sci.* **452** 322–36
Tozar A, Karahan I H and Yucel Y 2019 Optimization of the electrophoretic deposition parameters for biocomposite hydroxyapatite/chitosan/collagen/h-BN coatings on Ti6Al4V biomedical implants *Metallurgical and Materials Transactions a-Physical Metallurgy and Materials Science* **50A** 1009–20
Tudela I, Zhang Y, Pal M, Kerr I and Cobley A J 2015 Ultrasound-assisted electrodeposition of thin nickel-based composite coatings with lubricant particles *Surface & Coatings Technology* **276** 89–105
Unal E and Karahan I H 2018a Effects of ultrasonic agitation prior to deposition and additives in the bath on electrodeposited Ni-B/hBN composite coatings *J. Alloys Compd.* **763** 329–41
Unal E and Karahan I H 2018b Production and characterization of electrodeposited Ni-B/hBN composite coatings *Surface & Coatings Technology* **333** 125–37
Vitry V, Francq E and Bonin L 2019 Mechanical properties of heat-treated duplex electroless nickel coatings *Surf. Eng.* **35** 159–67
Waware U S, Hamouda A M S and Pradhan A K 2018 Effect of codeposition of mixed nanoparticles (V2O5 and ZrO2) on the structure and properties of Ni-B nanocomposite coating *J. Alloys Compd.* **752** 253–9
Yousif A, Kumar V, Jafer R M and Swart H C 2017 The effect of different annealing temperatures on the structure and luminescence properties of Y_2O_3:Bi^{3+} thin film fabricated by RF magnetron sputtering *Appl. Surf. Sci.* **424** 407–11